

# CW DFB RT diode laser-based sensor for trace-gas detection of ethane using a novel compact multipass gas absorption cell

Karol Krzempek · Mohammad Jahjah ·  
Rafał Lewicki · Przemysław Stefański ·  
Stephen So · David Thomazy · Frank K. Tittel

Received: 22 March 2013 / Accepted: 1 June 2013  
© Springer-Verlag Berlin Heidelberg 2013

**Abstract** The development of a continuous wave, thermoelectrically cooled (TEC), distributed feedback diode laser-based spectroscopic trace-gas sensor for ultra-sensitive and selective ethane ( $C_2H_6$ ) concentration measurements is reported. The sensor platform used tunable diode laser absorption spectroscopy (TDLAS) and wavelength modulation spectroscopy as the detection technique. TDLAS was performed using an ultra-compact 57.6 m effective optical path length innovative spherical multipass cell capable of 459 passes between two mirrors separated by 12.5 cm and optimized for the 2.5–4  $\mu m$  range TEC mercury–cadmium–telluride detector. For an interference-free  $C_2H_6$  absorption line located at  $2,976.8\text{ cm}^{-1}$ , a  $1\sigma$  minimum detection limit of 740 pptv with a 1 s lock-in amplifier time constant was achieved.

## 1 Introduction

Tunable diode laser absorption spectroscopy (TDLAS) is an important technique for the quantitative and sensitive detection of trace-gas molecules under various conditions. TDLAS requires a tunable laser device exhibiting single

frequency emission and a narrow linewidth at the targeted absorption line in order to achieve high sensitivity and selectivity of trace gas concentration measurements in the near and mid-infrared spectral range. TDLAS can be applied to real-time gas process applications [1, 2]. This work describes the use of an innovative ultra-compact multi-pass gas cell (MPC) and sensor control electronics board that were implemented in the reported  $C_2H_6$  trace gas sensor.

Detection of  $C_2H_6$  at low concentration levels is important in environmental monitoring [3, 4] and medical diagnostics [5, 6]. Moreover,  $C_2H_6$  is also recognized as an important greenhouse gas and its emission into the atmosphere by fossil fuel and biofuel consumption, biomass burning process and natural gas loss leads to long-term climate changes [7, 8].

In this paper, a spectroscopic trace-gas sensor based on a continuous wave thermoelectrically cooled, distributed feedback diode laser will be described. The CW TEC DFB diode laser emits in the 3.36  $\mu m$  wavelength range where an optimum  $C_2H_6$  absorption line can be detected. The sensor uses a second derivative wavelength modulation detection technique [9, 10]. Total dimensions of the employed multipass cell, the sensor control board (SCB), and the photodetector that compose the reported trace-gas sensor fulfill the requirements of a small in situ sensor system.

## 2 Experimental details

### 2.1 Sensor architecture

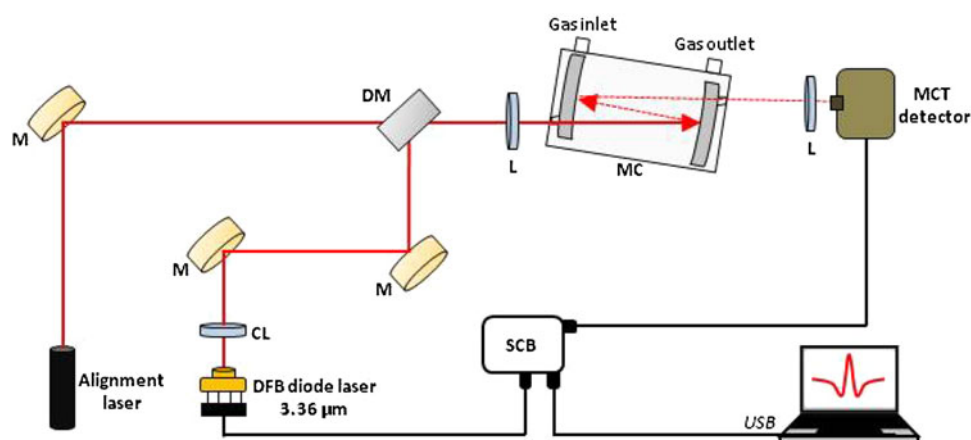
The  $C_2H_6$  sensor is depicted schematically in Fig. 1. A TEC CW GaInAsSb/AlGaInAsSb DFB diode laser (nanoplus S/N:891/2-17) emitting single-mode radiation in

K. Krzempek · P. Stefański  
Laser and Fiber Electronics Group, Wrocław University of  
Technology, Wybrzeże Wyspiańskiego 27, 50-370 Wrocław,  
Poland

M. Jahjah · R. Lewicki (✉) · P. Stefański · F. K. Tittel  
Department of Electrical and Computer Engineering, Rice  
University, 6100 Main Street, Houston, TX 77005, USA  
e-mail: rafal.lewicki@rice.edu

S. So · D. Thomazy  
Sentinel Photonics, 11 Deer Park Dr, STE 208,  
Monmouth Junction, NJ 08852, USA

**Fig. 1** Schematic of a  $C_2H_6$  gas sensor using a  $3.36\ \mu\text{m}$  DFB diode laser as an excitation source. *M* Mirror, *CL* collimating lens, *DM* dichroic mirror, *MC* multipass cell, *L* lens, *SCB* sensor control board



vicinity of  $2,977\ \text{cm}^{-1}$  ( $3.36\ \mu\text{m}$ ) was used as a convenient compact excitation source [10, 11]. The laser was packaged in a TO-5 that can be mounted inside an aluminum heat sink to provide sufficient heat dissipation. No additional air or water cooling was necessary when operating the laser diode at temperatures between 6 and  $16\ ^\circ\text{C}$ . The diode laser beam was collimated using a BlackDiamond™ aspheric lens (Thorlabs, model C036TME-E). Furthermore, a visible semiconductor diode laser beam ( $\lambda = 630\ \text{nm}$ ) was combined with the mid-IR beam by means of a dichroic mirror (ISP Optics, model BSP-DI-25-3) in order to simplify the optical alignment of the reported sensor architecture. Both laser beams were then focused into a novel 57.6 m optical pathlength spherical multi-pass gas absorption cell (Sentinel Photonics—[www.sentinelphotonics.com](http://www.sentinelphotonics.com)) using a 200-mm focal length plano-convex  $\text{CaF}_2$  lens (Thorlabs LA5714-E). The gas pressure inside the cell was set to 200 Torr by means of a pressure controller (MKS Instruments 649), which can also measure the  $C_2H_6$  flow with its embedded mass flow meter. After 459 passes in the MPC between two spherical mirrors separated by 13 cm, the output beam is focused onto a TEC mercury–cadmium–telluride (MCT) detector (VIGO PVI-4TE-4) using a 75-mm focal length plano-convex  $\text{CaF}_2$  lens (Thorlabs LA5042-E). The diode laser temperature and current control along with signal data acquisition are performed by a state of the art, compact electronics module (Sentinel Photonics). Data processing of the  $2f$   $C_2H_6$  absorption signal was carried out by a dedicated LabVIEW program.

## 2.2 Laser source parameters

The CW DFB diode laser can target the Q-branch feature ( $P_{Q_3}$ ) of the  $\nu_7$   $C_2H_6$  band located at  $2,976.8\ \text{cm}^{-1}$ . At this wave number, the diode laser emits 1.75 mW of single-mode radiation, as measured after the collimating lens, when the diode laser temperature and current were set to  $6\ ^\circ\text{C}$  and 170 mA, respectively. By varying the diode laser

temperature from 6 to  $16\ ^\circ\text{C}$ , the frequency of the emitted laser radiation was tuned between  $2,975.3$  and  $2,978.9\ \text{cm}^{-1}$ , maintaining a stable, single-mode operation [10]. The calculated current and temperature tuning coefficients of the used DFB diode laser are  $-0.022\ \text{cm}^{-1}/\text{mA}$  and  $-0.26\ \text{cm}^{-1}/^\circ\text{C}$ , respectively.

## 2.3 Novel spherical multipass cell

A novel ultra-compact, dense patterned multi-pass gas absorption cell, which uses a spherically aberrated 2-mirror configuration to obtain a 57.6 m effective optical path length, is depicted in Fig. 3. The MPC design allows 459 passes across a pair of 40-mm diameter mirrors with minimal spot overlap to reduce etalon fringe effects. Moreover, the MPC has a footprint (excluding fittings) of  $17\ \text{cm} \times 6.6\ \text{cm}$  and a total sampling volume of 270 cm which significantly reduces the gas sampling time as compared to traditional MPCs when performing  $C_2H_6$  concentration measurements. The mirrors were dielectric-coated spherical glass substrates, providing  $>99.8\ \%$  reflectivity in the selected  $3.36\ \mu\text{m}$  spectral region. Although the MPC is constructed similarly to a spherical Herriott cell with two coaxial spherical mirrors [12, 13], the aberrated configuration allows for spot patterns which are not simply a circle or ellipse (Fig. 3). The cell configuration was determined using artificial intelligence optimization of the ray tracing results. The optimization routine varied the entrance angle of entrance, beam entrance location, and physical distance between the MPC mirrors. The parameters which were optimized were the overall path length, inter-spot distance, and exit-hole-distance relative to other spots. Such a MPC has a significant advantage in terms of cost compared to traditional astigmatic Herriott MPCs, due to the use of standard concave spherical mirrors. The manufacturing tolerance of such spherical mirrors is much easier to achieve than astigmatic mirrors. This MPC also provides an advantage in terms of spot focusing. Cylindrical mirrors can only focus the beam in one

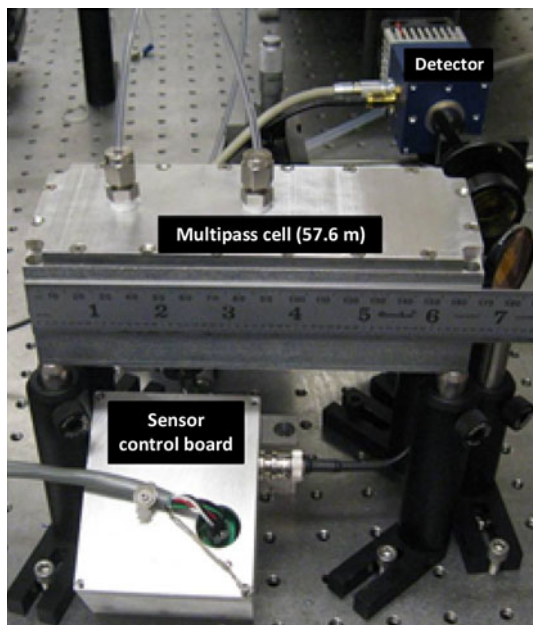


**Fig. 2** Photograph of the novel spherical compact multipass gas absorption cell and the SCB, enclosed in a custom aluminum case

direction for a single transit, while a spherical/astigmatic spherical mirror can focus in two directions. The main issue with spherically aberrated MPCs is that the aberration slowly increases with each pass, causing the spot to change into an ellipsoid with each transit. However, as long as the spot exits and the radiation can be collected by the detector, this issue does not affect the sensor performance. The MPC used two wedged  $\text{CaF}_2$  windows for light injection/extraction from the cell. The wedges were oriented to prevent standing wave reflections, which can lead to etalon fringes that would be detrimental to detection sensitivity. Furthermore, the window assembly design permits the sealing of the MPC for low-pressure operation in conjunction with pressure fittings and rubber o-rings.

#### 2.4 Sensor control electronics

The diode laser control electronics is embedded in the SCB as shown in Figs. 1 and 2. The SCB based on a Texas Instruments processor (TI MSP430) provides temperature control via thermistor sensing and a power output which can drive the TEC of the laser diode. The control electronics directly controls the laser diode drive current and produces modulation of the current to perform TDLAS measurements using wavelength modulation spectroscopy as a detection technique. An embedded analog-to-digital converter samples the data synchronously, and a 32-bit digital lock-in amplifier algorithm produces characteristic absorption spectra when performing wavelength modulation. Sawtooth current ramping is also driven synchronously by the processor. The output from the SCB board is

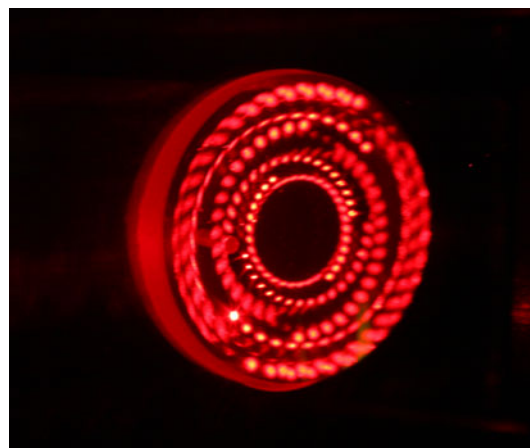


**Fig. 3** Photograph of the multipass gas absorption cell beam pattern visualized by using a visible (650 nm) trace diode laser beam

a continuous sawtooth ramp spectrum at 8 Hz. The total control and data acquisition systems power consumption to generate wavelength modulated ramp spectra were  $<0.4$  W. The SCB measures  $70 \text{ mm} \times 50 \text{ mm} \times 10 \text{ mm}$  and is placed inside a custom enclosure as depicted in Fig. 3. The SCB has an USB output which sends the sensor data to a LabVIEW interface. The data rate of the USB output has a maximum of 2 Mbps, but was set to 1 Mbps in order to minimize the digital noise emission. The SCB drives the laser diode TEC with a bi-directional switched-mode output to reduce power consumption by increasing the power efficiency. The bi-directional output allows both heating and cooling by means of the TEC. The switching frequency was set to 500 kHz with a 15 kHz filter for smoothing. Typical characteristics of the SCB used in this work are as follows: (1) a digital temperature controller with a typical noise level of 0.001 K, (2) a switch-mode TEC drive current up to 1 A, (3) a laser diode compliance voltage/current of 3 V/0.3 A, and (4) a typical noise equivalent absorption level of  $10^{-5}$  in the  $2f$  mode.

### 3 Measurements and results

The HITRAN database [14] simulation plot for absorption spectra of the targeted  $\text{C}_2\text{H}_6$  line, along with  $\text{CH}_4$  and 2 %  $\text{H}_2\text{O}$ , can be found in a previously reported work [10]. The targeted  $\text{C}_2\text{H}_6$  rotational-vibrational absorption line at  $2,976.8 \text{ cm}^{-1}$  is interference free from other molecules observed in ambient air (such as  $\text{H}_2\text{O}$ ,  $\text{CO}_2$ ,  $\text{CH}_4$ ).

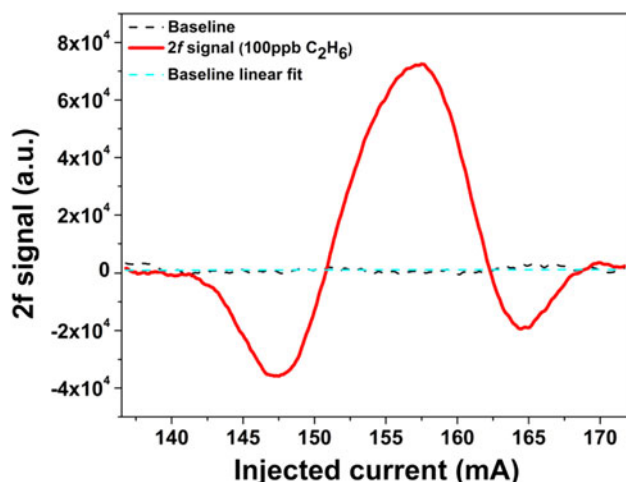
#### 3.1 Measurement of $\text{C}_2\text{H}_6$ sensor system parameters

Ethane sensor evaluation and calibration measurements were performed using a  $2f$  WMS detection technique [15] and a certified cylinder containing a 100 ppb  $\text{C}_2\text{H}_6:\text{N}_2$

mixture. In order to target the desired  $C_2H_6$  absorption line, the laser temperature and current were set to 9.5 °C and 136.7 mA, respectively. To perform a wavelength scan across the targeted  $C_2H_6$  absorption line, an 8 Hz sawtooth current ramp corresponding to an effective frequency scanning range of  $0.11\text{ cm}^{-1}$  was applied to the diode laser. In addition, a 16-kHz sinusoidal modulation signal with an amplitude of 15.6 mA was superimposed on the ramping signal. The modulation depth and gas pressure were evaluated experimentally in order to achieve the maximum  $2f$   $C_2H_6$  signal amplitude. A pressure of 200 Torr inside the MPC was found to provide optimal measurement conditions. A narrow current scanning range ensured low laser temperature fluctuations, therefore, limiting the electrical noise introduced to the  $C_2H_6$  sensor measurements.

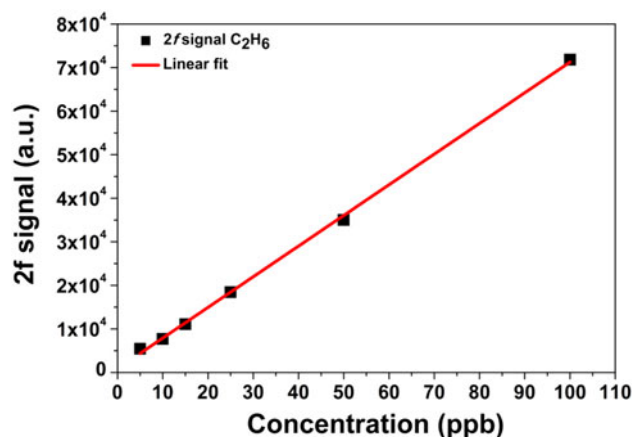
### 3.2 Results

Figure 4 depicts the acquired 100 ppbv  $C_2H_6$   $2f$  signal at 200 Torr and the baseline measured after flushing the MPC with pure nitrogen. For a 57.6 m effective optical path-length and  $\sim 1$  s sample averaging time, the calculated signal-to-noise ratio was  $\sim 135$ , yielding a minimum detectable  $C_2H_6$  concentration of 740 pptv ( $1\sigma$ ). High detection resolution was a combined result of using a state-of-the-art SCB shielded with an aluminum casing along with a sensitive (10 V peak-to-peak signal amplitude), low noise mid-IR VIGO detector with a detectivity  $D^*$  of  $>1 \times 10^{11}\text{ cm Hz}^{1/2}/\text{W}$ . The dependence of the  $2f$  signal as a function of  $C_2H_6$  concentration is plotted in Fig. 5. The linear response of the  $C_2H_6$  sensor system to  $C_2H_6$  concentration variations was confirmed by fitting the data with a linear slope. For actual in situ ambient air



**Fig. 4**  $2f$  WMS signal for a  $C_2H_6$  absorption line located at  $2,976.8\text{ cm}^{-1}$  (pressure = 200 Torr)

measurements, the  $H_2O$  absorption line overlaps with the targeted  $C_2H_6$  line and becomes dominant when  $C_2H_6$  concentration drops below 10 ppbv. To eliminate atmospheric water vapor interference on the measured  $C_2H_6$  signal, an additional dehumidification system can be added in line at the inlet to the sensor system. Additionally, Allan variance measurements were performed to determine the stability and resolution of the reported  $C_2H_6$  sensor system. The Allan deviation plot, depicted in Fig. 6, was determined by measuring and averaging the  $2f$  TDLAS signal corresponding to the absorption of 100 ppbv of  $C_2H_6$ . The stability of the sensor system in a free running non-wavelength locked mode allows averaging up to 35 s derived from the Allan deviation plot. The initial rise for Allan plot is caused by averaging the acquired  $2f$  spectra. This is the direct result of the filter time constant reduction in the short-term noise present in the acquired data [16]. During



**Fig. 5** Linear dependence of the measured  $2f$  TDLAS signal as a function of the  $C_2H_6$  concentration

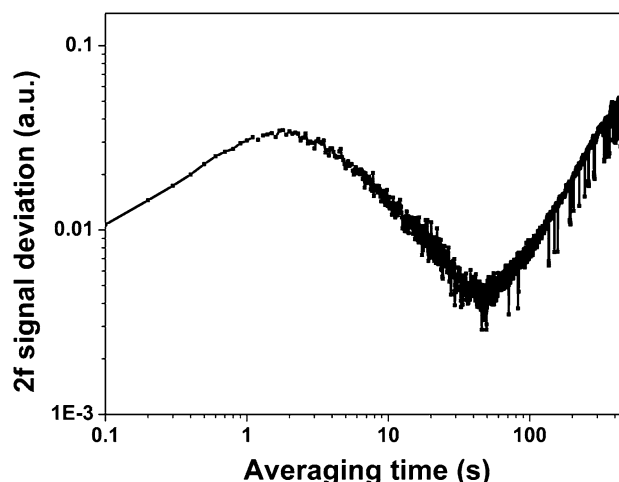


**Fig. 6** Measured Allan deviation for the  $2f$  TDLAS signal corresponding to the absorption of 100 ppbv of  $C_2H_6$

a 3 weeks measurement period, it was not necessary to adjust the laser diode current set point or the TEC temperature in order to keep the targeted  $C_2H_6$  absorption line within the 30 mA of applied current scanning range. Using the same measurements conditions (e.g. injected current, temperature) it is possible to keep the position of the targeted  $C_2H_6$  line peak fixed with estimated current drift less than  $\pm 2$  mA. A reference channel for synchronous absorption line locking can be added in a future version of the reported  $C_2H_6$  sensor system.

#### 4 Conclusions

Experiments incorporating a novel spherical 57.6 m optical path MPC and integrated control and data processing electronic module for the detection of  $C_2H_6$  trace concentrations are reported. In order to achieve sub-ppb level  $C_2H_6$  concentration measurements, a TDLAS  $2f$  wavelength modulation technique was applied to an interference-free absorption line located at  $2,976.8\text{ cm}^{-1}$ . The  $1\sigma$  minimum detection limit is 740 pptv when a 1 s sample averaging time is used. By using a state-of-the-art sensitive photovoltaic MCT detector and integrated electronics, significant noise reduction and signal quality were achieved. A further improvement of the reported  $C_2H_6$  sensor will include implementing absorption line-locking functionality in the control software and further miniaturization of the sensor architecture that will result in an ultra-compact, robust, and portable sub-ppb level  $C_2H_6$  sensor platform.

**Acknowledgments** The Rice University group acknowledges the financial support from a National Science Foundation (NSF)

Engineering Research Center sub award for “Mid-infrared Technologies for Health and the Environment (MIRTHE)” from Princeton University, a NSF International Collaboration in Chemistry award: NexCILAS CHE-1124577 and grant C-0586 from The Welch Foundation. The development of the laser diode was supported by the European Commission within the project SensHy 223998 of the 7th Framework Program. The laser diode was fabricated by nanoplus GmbH, Germany.

#### References

1. S.G. So, D. Chang, O. Al'Rifai, G. Wysocki, A.A. Kosterev, F.K. Tittel, CLEO/QELS (2008)
2. C.J. Smith, S. So, G. Wysocki, CLEO/QELS (2010)
3. B. Hirst, G. Gibson, S. Gillepsie, I. Archibald, O. Podlaha, K.D. Skeldon, S. Monk, M. Padget, Atmos. Environ. **41**, 1128 (2007)
4. G. Etiope, P. Ciccioli, Science **323**(5913), 478 (2009)
5. C. Wang, P. Sahay, Sensors **9**, 8230–8262 (2009). doi:10.3390/s91008230
6. S. Kanoh, H. Kobayashi, K. Motoyoshi, Chest **128**(4), 92–2387 (2005)
7. Y. Xiao, J.A. Logan, D.J. Jacob, R.C. Hudman, R. Yantosca, J. Geophys. Res. **113**, D21306 (2008)
8. I.J. Simpson, M.P. Andersen, S. Meinardi, L. Bruhwiler, N.J. Blake, D. Helmig, F.S. Rowland, D.R. Blake, Nature **488**, 490–494 (2012)
9. J.A. Silver, Appl. Optics **31**(6) (1992)
10. K. Krzempek, R. Lewicki, L. Nähle, M. Fischer, J. Koeth, S. Belahsene, Y. Rouillard, L. Worschech, F.K. Tittel, Appl. Phys. B **106**, 251–255 (2012)
11. W. Zeller, L. Naehle, P. Fuchs, F. Gerschuetz, L. Hildebrandt, J. Koeth, Sensors **10**, 2492–2510 (2010)
12. S. So, D. Thomazy, CLEO 2012: Science and innovations, CW3B (2012)
13. G.S. Engel, E.J. Moyer, Opt. Lett. **32**(6), 704–706 (2007)
14. <http://www.cfa.harvard.edu/hitrans>
15. S. Schilt, F.K. Tittel, K.P. Petrov, Encycl. Analyt. Chem. (2011). doi:10.1002/9780470027318.a0707.pub2
16. P. Werle, Appl. Phys. B **102**, 313–329 (2011)